Organic molecular beam deposition: fundamentals, growth dynamics, and *in situ* studies

2008 J. Phys.: Condens. Matter 20 184005

(http://iopscience.iop.org/0953-8984/20/18/184005)

IOP PUBLISHING JOURNAL OF PHYSICS: CONDENSED MATTER

J. Phys.: Condens. Matter **20** (2008) 184005 (12pp) doi:10.1088/0953-8984/20/18/184005

Organic molecular beam deposition: fundamentals, growth dynamics, and *in situ* studies

S Kowarik, A Gerlach and F Schreiber

Institut für Angewandte Physik, Universität Tübingen, Auf der Morgenstelle 10, 72076 Tübingen, Germany

Received 4 September 2007, in final form 5 November 2007
Published 17 April 2008
Online at stacks.iop.org/JPhysCM/20/184005

Abstract

We review recent progress on thin film growth by organic molecular beam deposition (OMBD). We give a brief overview of growth physics with emphasis on the specific characteristics of organic materials, such as weak van der Waals binding forces and conformational and orientational degrees of freedom of the molecular building blocks. Two recent developments in experimental studies of OMBD will be discussed in more detail: (1) we will give examples for *real-time and in situ* growth studies during deposition of the organic semiconductors pentacene, diindenoperylene, and PTCDA and (2) we will give an overview of high precision *in situ* investigations of the first molecular monolayer, in particular using the x-ray standing wave technique.

(Some figures in this article are in colour only in the electronic version)

1. Introduction

The strong increase in research activity on organic thin films is to a large extent, although not exclusively, motivated by the perspectives of and in some cases already realized applications in various areas including electronics and optoelectronics. Some examples for these are included also in other reviews in this special issue [1]. At the same time, it has also been recognized that the performance of devices is intimately coupled to the structural characteristics. The understanding of growth is therefore mandatory to improve and control devices.

In this review we focus on organic molecular beam deposition (OMBD), i.e. evaporation of the molecules, usually in ultrahigh vacuum (UHV). OMBD is the typical method of thin film preparation for small molecule organic semiconductors because they often exhibit only low solubility, while growth from solution (e.g. spin coating, inkjet printing, and spray coating) enjoys great popularity in particular for polymeric systems. We should note that there is also the term organic molecular beam epitaxy (OMBE) [2], but we consider OMBD as the more general term, since it also includes systems without epitaxial relation to the substrate. From a fundamental perspective, it has been realized that OMBD exhibits its own specifics different from growth of atomic systems, e.g. changes of molecular conformation during growth [3], large thermal expansion coefficients [4] or an additional source of disorder due to molecular tilt domains [5]. The orientational/tilt degrees of freedom of molecules probably are the most important difference to atomic systems, and imply that the problem is generally anisotropic, and that not only the positional adsorption state of a molecule, but also its orientation must be considered [6, 7].

The present review is concerned with some general aspects of OMBD and also a few recent results. We will discuss

- typical systems;
- general principles of growth;
- specific characteristics of organics;
- some examples/brief overview of growth behaviour.

We will focus in particular on two recent developments, namely

(i) real-time studies of organic thin film growth, an important development to reveal transient structures, that can modify the growth behaviour, and

(ii) high resolution studies of the molecular adsorption geometry, which not only influences the growth of the subsequent layers, but also has a strong impact on the charge carrier (electron or hole) injection from metallic contacts into organic semiconductors, which can easily be seen from the dependence of injection on distance and also from the (possibly

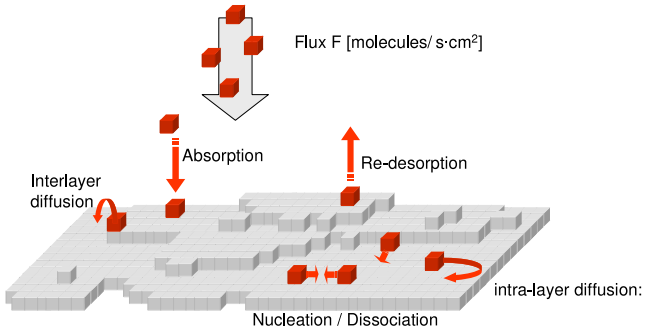

Figure 1. Schematic of atomistic processes relevant for OMBD.

induced) interface dipole upon adsorption (possibly enhanced by molecular bending) [1, 8–10].

In a review with limited space such as the present one, we of course cannot give an exhaustive overview for which we refer to earlier reviews [11–17]. Instead, the examples are centred mostly on our own work, which we will discuss in a broader context.

2. Some general considerations of growth

Growth of crystalline thin films is an enormously rich subject with many different facets and theoretical approaches, e.g. equilibrium considerations about crystal phases and shapes, statistical analysis of correlation lengths and surface roughness, or detailed analysis of dynamic processes of growth like diffusion and nucleation (see figure 1). A thorough treatment of its theoretical aspects can be found in [18–21]. Here we want to briefly touch the aspects of the in plane crystallographic relationship, the out of plane structure/evolution of morphology, as well as dynamic scaling before discussing specific issues of organic thin film growth.

It is important to realize that a description of these aspects cannot solely rely on thermodynamic arguments (by which we mean static, equilibrium considerations), but also kinetic aspects of OMBD and its irreversible atomic scale processes (see figure 1) must be taken into account [22–25]. The growth of organic molecular films often leads to non-equilibrium structures due to the growth kinetics as can be seen from significant post-growth re-organization [26–28].

2.1. Epitaxy/in plane crystallographic relationship

We will not discuss in great detail the issues related to epitaxial relations, that is the crystallographic relation between film and substrate, as some of our examples deal with relaxed polycrystalline growth on amorphous substrates. For growth on crystalline substrates, we want to point out that the strain induced by the lattice mismatch at the film substrate interface is not only important in a crystallographic sense [2], but also influences the growth beyond the structure of the first monolayer. For example it has been shown that diindenoperylene (DIP) grown on NaCl single crystals exhibits herringbone type packing, but when DIP is grown on crystalline perylene thin films an unusual sandwich herringbone type packing is observed [29]. This suggests, that by careful selection of the (organic) substrate the crystal structure of epitaxial adlayers can be controlled not only in the first monolayer adjacent to the substrate, but also in following monolayers. In this respect the first monolayer is the most important one, determining the crystal structure of an entire multilayer film. For details on organic epitaxy see the review by Hooks *et al* [30].

2.2. Overall structure (out of plane)/evolution of morphology

In general one can distinguish the three growth scenarios depicted in figure 2: island (Volmer–Weber), layer-plus-islands (Stranski–Krastanov), and layer-by-layer growth (Frank–van der Merwe). Typically, the surface energies $\gamma_{\text{substrate}}$, γ_{film}, and $\gamma_{\text{interface}}$ (see figure 2) are related to these growth modes using energetic (equilibrium) arguments.

Note that the modification of the substrate surface energy to change the growth behaviour of the OMBD film has enjoyed some popularity. The most important strategy is based on the use of self-assembled monolayers [13, 31]. Early work demonstrated the use of alkanethiol SAMs on Au(111) to modify PTCDA growth [31–33]. In the context of pentacene growth this strategy has been very successful [34–37], although it is not always obvious which feature of the SAM exactly leads to the modification of the growth of the subsequent film. A detailed discussion of this approach, however, is beyond the scope of this review.

In particular the layer-plus-island growth mode is typical for organic systems, as exemplified by PTCDA on Ag(111) in this review. The examples of real-time growth studies in section 3 demonstrate that by measuring the out of plane morphology during growth one can readily distinguish growth modes as well as measure threshold thicknesses where the growth behaviour changes.

For a more detailed description in a given growth scenario, one must use an additional growth model to quantify properties such as island size or film roughness and their evolution with film thickness. For island growth that leads to roughening of the film surface, rate equation models encompassing microscopic processes like interlayer diffusion (see figure 1) can be used [38]. In cases with little knowledge of atomic processes, the roughness evolution can be more generally expressed in terms of growth exponents as discussed in the next section [39, 40].

2.3. Dynamic scaling

An important concept for the theoretical description of growth is based on dynamic scaling [39–41]. During the last two decades a theoretical framework for relating growth mechanisms to a set of scaling exponents has been developed, and there have been significant efforts to theoretically predict and experimentally determine scaling exponents for certain growth modes.

The film morphology can be described by scaling theory using three parameters for the typical surface slope a, the correlation length ξ beyond which the heights at two points become uncorrelated, and the standard deviation of the film

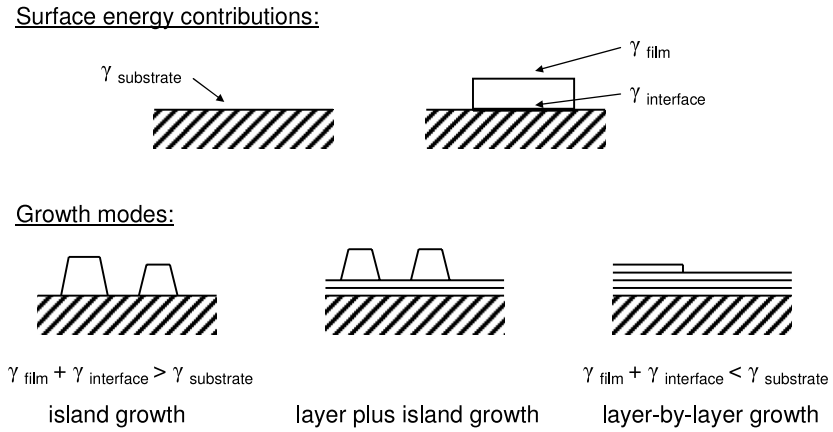

Figure 2. Scenarios for thin film growth: depending on the material specific surface free energies three different generic growth modes are generally distinguished: island growth, layer plus island growth, and layer-by-layer growth.

height σ (rms roughness)[1]. These parameters scale with film thickness D according to $a \sim D^{\lambda}$, $\xi \sim D^{1/z}$, $\sigma \sim D^{\beta}$, defining the steepening exponent λ, the dynamic exponent z, and the growth exponent β.

For organics, there are only few studies available. Interestingly, both DIP on silicon oxide as well as phthalocyanines [42] seem to display significant roughening parameters (high β). Values of the roughening parameter $\beta > 0.5$ indicate rapid roughening faster as expected for random deposition in a 'hit-and-stick' model. Rapid roughening has been measured for DIP/SiO_2 ($\beta = 0.748 \pm 0.05$), H_2Pc/glass ($\beta = 1.02 \pm 0.08$), and plasma polymer ($\beta = 0.7 \pm 0.10$) [42], but the effect is also found in inorganic materials [43].

2.4. Issues specific for growth of organic molecular materials

The general considerations above apply both to organic and inorganic materials, but several aspects specific to organic materials can lead to distinctively different growth behaviour.

(i) As extended objects, organic molecules have internal degrees of freedom. The *vibrational degrees of freedom* can impact the interaction with the substrate and also the thermalization upon adsorption on the surface, because the translational energy of a molecule can also be converted to internal vibrational energy. *Conformational degrees of freedom* mean that the building block can change within the film, for example by bending to accommodate stress. The conformation of the organic semiconductor rubrene has been found to change during growth [3], which may influence the film morphology [44]. *Orientational degrees of freedom* which are not included in conventional growth models can give rise to tilt domains and thereby an additional source of disorder, or may even give rise to 'lying down' and 'standing up' structures [6, 35] as discussed later for the example of DIP.

(ii) The interaction between molecules and between molecules and the substrate is often dominated by weak van der Waals forces. It is important to emphasize that when integrated over all atoms within a molecule, the weak interaction energies add up and lead to substantial molecular binding energies in the eV range. Nevertheless the weaker interactions per atom lead to 'softer' materials and, for example, strain can be accommodated more easily. Due to the weaker interactions the thermal expansion coefficients (typically in the 10^{-4} K^{-1} range) are large when compared to inorganic materials, which possibly leads to higher thermally induced strain at film–substrate interfaces.

(iii) The size of the molecules and consequently the size of the unit cell is larger than that of inorganic materials, and therefore the interaction potential is spread out over a larger area. This weakens the effective substrate corrugation as experienced by molecules because the small length scale substrate corrugation is averaged to some extent over the size of the molecule which in general has inter-atomic bond lengths different from the substrate. Also more translational and orientational domains for epitaxy on inorganic substrates are possible due to the difference in unit cell size. This introduces an additional source of disorder for organics.

3. Real-time and *in situ* growth studies

With this review we build on previous reviews [11–17] and therefore will focus on recent work on *real-time* and *in situ* growth studies. *In situ* techniques for monitoring organic molecular beam deposition offer great advantages because post-growth sample changes such as oxidation or dewetting do not obscure the results, and, given a time resolution matching the growth processes they also allow one to follow details of growth in *real time* during the deposition process. There exist a number of surface sensitive *in situ* techniques with real-time capability such as low energy electron microscopy [45],

[1] The parameters are defined using the height difference correlation function (HDCF) $g(R) = \langle [h(x, y) - h(x', y')]^2 \rangle$ of two points laterally separated by $R = \sqrt{(x - x')^2 + (y - y')^2}$. The HDCF displays distinct behaviours for $R \ll \xi$ and $R \gg \xi$, where ξ denotes a correlation length. For $R \ll \xi$ one expects a power law increase as $g(R) \approx a^2 R^{2\alpha}$, where α is the static roughness exponent and the prefactor a is a measure of the typical surface slope. For $R \gg x$ the heights at distance R become uncorrelated. Hence $g(R)$ saturates at the value $g(R) = 2\sigma^2$, where $\sigma = \sqrt{\langle (h - \langle h \rangle)^2 \rangle}$ is the standard deviation of the film height (or 'rms roughness').

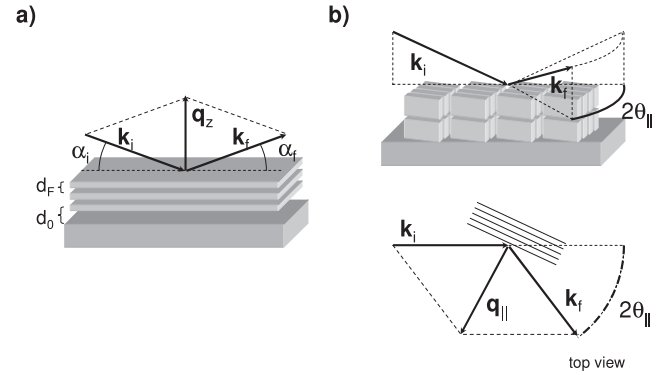

Figure 3. (a) Scattering geometry for specular x-ray reflectivity measurements, revealing the sample structure (roughness, lattice spacing) along the surface normal. (b) Scattering geometry for grazing incidence diffraction, which measures lattice constants parallel to the sample surface.

reflection high energy electron diffraction (RHEED) [46], or helium scattering [47, 48]. Here we focus on x-ray scattering, which offers flexibility in sample environment (vacuum/air/liquids/penetration of thin solids), offers high spatial resolution and can be analysed in most cases by a simple single scattering (kinematic) theory.

Two x-ray scattering geometries are depicted in figures 3(a) and (b), which are used to determine the sample structure along the surface normal and parallel to the sample surface respectively. In x-ray reflectivity measurements the wavevector changes by q_z upon reflection and a layering along the surface normal (in the direction of q_z) will lead to a Bragg reflection. Similarly for grazing incidence diffraction lattice spacings within the plane can be calculated from the position of Bragg reflections where the wavevector transfer $q_{||}$ is parallel to the sample plane. These two scattering geometries will be applied in the following to study the structural evolution during thin film deposition.

3.1. Pentacene/silicon oxide

Pentacene is attracting considerable attention as its charge transport properties are excellent [16, 49], and films of pentacene on silicon oxide are commonly used for thin film transistors in which the silicon oxide serves as gate dielectric.

Its thin film structure on silicon oxide (see e.g. [50]) as well as modified silicon surfaces [36] has been studied extensively, for details we refer to [51] and references therein. Recently the molecular arrangement within the unit cell has been solved experimentally for silicon oxide [52, 53] as well as octadecyltrichlorosilane-treated silicon oxide [53]. A dynamic scaling analysis of the island distribution in sub-monolayer films shows that islands containing three or more molecules are stable [41, 54]. A comparison of hydrophilic, oxidized silicon substrates with hydrophobic H-atom terminated silicon substrates has shown that with increasing hydrophobicity the nucleation density of pentacene islands decreases by a factor of 100 while the island size increases [36]. Under optimized conditions the island size in pentacene thin films can be as large as 0.1 mm as demonstrated in [45]. In addition to varying substrate temperature and deposition rate, the kinetic energy of pentacene molecules has been varied in supersonic beam deposition [34, 47, 55]. Increasing the kinetic energy of pentacene molecules from 1.5 to 6.7 eV the adsorption probability decreases by a factor of ∼5, indicative of trapping-mediated adsorption [55].

Using real-time techniques, the evolution of different pentacene phases during growth [56], dendritic island shape [45], the coverages of individual layers [57–59], or the Ehrlich–Schwoebel barrier [58] can be studied. Real-time measurements of the x-ray reflectivity (as shown in figure 4(b)), allow one to determine the crystal structure(s) from the positions of the Bragg reflections, and also the evolution of the interface width (roughness) of the film can be extracted. In [56] it was shown that the nucleation of a second pentacene phase [50, 51, 60] occurs as early as the first pentacene monolayer as determined from following the Bragg reflections corresponding to the two phases.

From the data in figure 4 as well as grazing incidence diffraction data [59], it can be seen that only the so called thin film phase of pentacene with an out of plane lattice constant of 15.6 Å is growing for the conditions employed, as opposed to the pentacene bulk phase with a lattice constant of 14.5 Å [51]. Analysing not only the Bragg reflections, but also the evolution of the reflectivity between the Bragg reflections, additional information can be learned. Halfway between the Bragg reflections at the so called anti-Bragg point the interference of x-rays scattered from neighbouring layers interferes destructively, leading to an oscillating x-ray reflectivity when subsequent pentacene layers are filled. From these oscillations the number of pentacene monolayers that have been grown can be directly counted (oscillation period two monolayers). As can be seen from figure 4 the x-ray reflectivity shows modulations not only at the anti-Bragg condition, but also at all q-values other than the Bragg condition. These growth oscillations at several q-points correspond to several Fourier components of the real-space structure and therefore it is advantageous to measure the reflectivity in a wide q-space region (0.25–0.8 Å^{-1} in this case) to get a precise measurement of the real-space structure and the film roughness [61]. The growth oscillations can be described theoretically by the following equation (1), which includes the scattering from the substrate as well as the sum over the scattering of every individual pentacene layer:

$$I_{\text{reflected}}(q,t) = \left| A_{\text{substrate}}(q) \mathrm{e}^{\mathrm{i}\Phi(q,d_0)} + f(q) \sum_n \theta_n(t) \mathrm{e}^{\mathrm{i}nqd_{\text{F}}} \right|^2 . \quad (1)$$

$A_{\text{substrate}}(q)$:	substrate scattering amplitude;
$f(q)$:	molecular form factor of pentacene;
$\Phi(q, d_0)$:	phase between substrate and adlayer scattering;
n:	layernumber;
θ_n:	fractional coverage of the nth layer (0—zero coverage, 1—filled layer);
q:	x-ray wavevector transfer upon reflection;
d_{F}:	lattice spacing within the crystalline thin film.

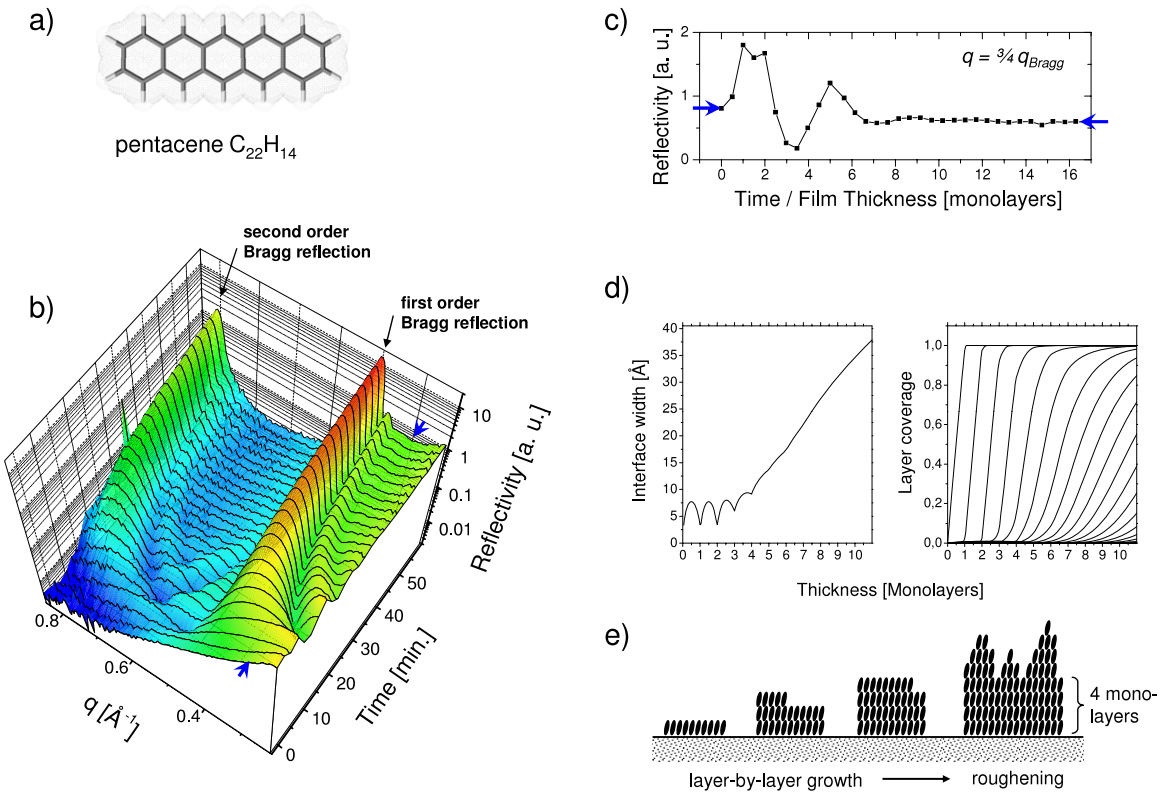

Figure 4. (a) Schematic of the pentacene molecule. (b) Real-time measurements of the x-ray reflectivity in a wide q-range during pentacene deposition on silicon oxide have been performed at the EDR beamline at BESSY II (deposition rate 3.5 Å min^{-1}, substrate temperature 50 °C). Two peaks corresponding to the first and second order Bragg reflection of the pentacene thin film phase can be seen to grow with increasing deposition time (from [59] with permission). (c) Example of a growth oscillation at $q = 3/4\ q$ Bragg as a cut through the data set in (b), as indicated by the arrows. (d) Using a diffusive growth model and the kinematic approximation in x-ray scattering (see text) the interface roughness of the pentacene film and the coverage of individual layers during growth can be extracted from the data set in (b). (e) From the evolution of the surface roughness it can be seen that layer-by-layer growth persists for the first four monolayers before roughening sets in.

To describe the time evolution of $\theta_n(t)$ in equation (1) a range of growth models can be used [19, 62, 63]. A simple model that can describe the experimental growth oscillations is a diffusive growth model (equation (2), see [62]) where the rate for a jump from layer $n+1$ to n is proportional to the uncovered fraction of layer $n+1$ (i.e. how many molecules in layer $n+1$ are not buried and free to move) and the available space in layer n (i.e. uncovered space on top of layer $n-1$):

$$\frac{\mathrm{d}\theta_n}{\mathrm{d}\,(t/\tau)} = (\theta_{n-1} - \theta_n) + k_n(\theta_{n+1} - \theta_{n+2})(\theta_{n-1} - \theta_n) - k_n(\theta_{n-2} - \theta_{n-1})(\theta_n - \theta_{n+1}). \quad (2)$$

θ_n: fractional coverage of the nth layer;
τ: completion time for one monolayer;
k_n: effective rate for interlayer transport.

Using equation (2) to calculate the $\theta_n(t)$ and inserting them in equation (1) yields theoretical growth oscillations which can be made to fit experimental values by adjusting the rate constants k_n. The solutions $\theta_n(t)$ of equation (2) are S-shaped curves as shown in figure 4(d).

The $\theta_n(t)$ contain the complete information about the out of plane film structure, and as a measure of the film roughness the interface width can be derived from them. The film roughness or interface width is defined as the standard deviation of the interface from the average film thickness:

$$\text{interface width} = \sqrt{(1-\theta_1)(0-\bar{d})^2+(\theta_1-\theta_2)(1-\bar{d})^2+(\theta_2-\theta_3)(3-\bar{d})^2+\cdots} \quad (3)$$

interface width: in units of the step height of one monolayer;
$\bar{d}$: average film thickness units of the step height of one monolayer.

For pentacene, the roughness data shows a clear change in growth mode after four monolayers. While the growth oscillations in the beginning show that pentacene grows in a layer-by-layer fashion (with an oscillating surface roughness), after four monolayers the surface width starts to increase. This change in growth mode from layer-by-layer growth to roughening has also been observed in [57, 58], where the interlayer transport of pentacene molecules could be quantified. While the exact nature of this transition is unknown, several factors may contribute such as decreased interlayer transport (increasing Schwoebel barrier), faster nucleation, and decreased diffusivity on top of islands.

3.2. DIP/silicon oxide

Diindeno(1,2,3,-cd,10,20,30-lm)perylene (C32H16, DIP, a red dye, figure 1(a)) is less popular than pentacene, but its growth

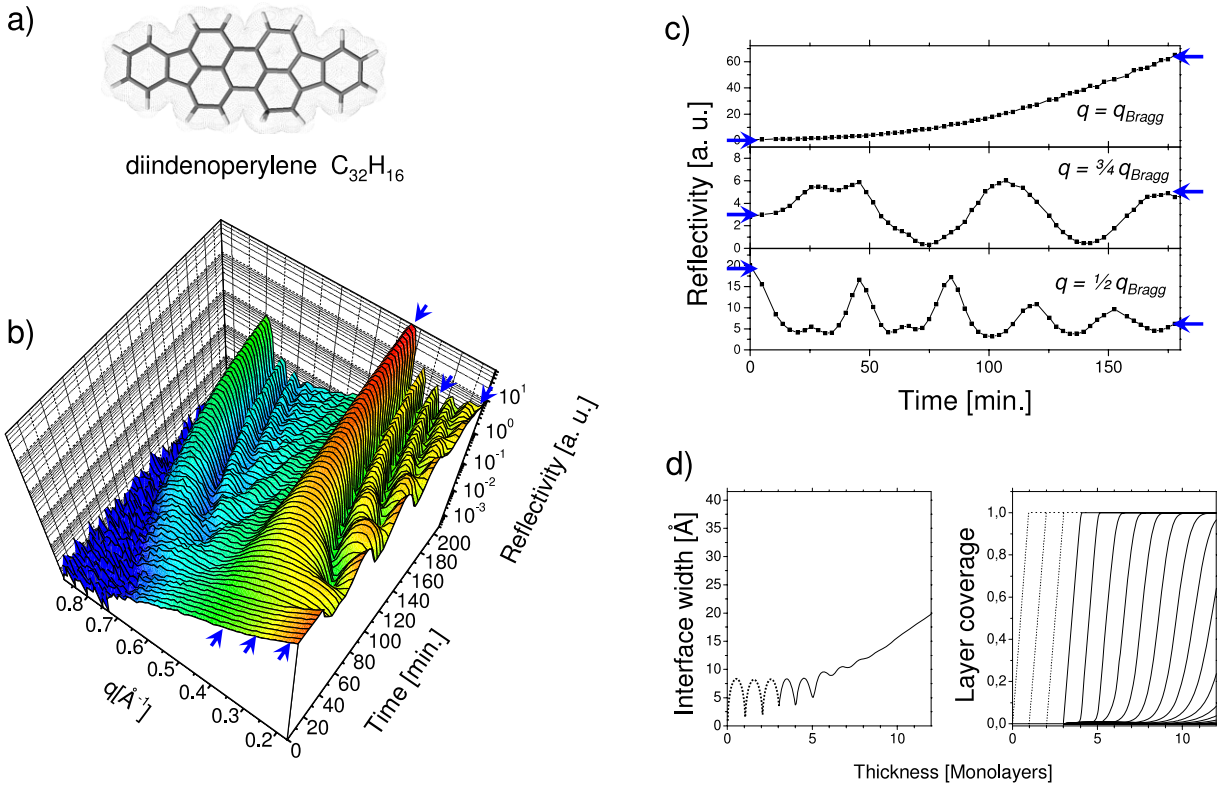

Figure 5. (a) Schematic of the diindenoperylene (DIP) molecule. (b) Real-time measurements of the x-ray reflectivity in a wide q-range during DIP deposition on silicon oxide have been performed at beamline ID10B at the ESRF (deposition rate 0.6 Å min^{-1}, substrate temperature 130 °C). Two peaks corresponding to the first and second order Bragg reflection of DIP can be seen to grow with increasing deposition time. (c) Cuts through the data set in (b) show an oscillating x-ray reflectivity at the anti-Bragg condition and the Bragg condition, while at the Bragg condition the reflectivity increases monotonically. Using a diffusive growth model and the kinematic approximation in x-ray scattering (see text) the growth oscillations can be fitted (solid line). (d) From the fit of the growth oscillations the interface roughness of the DIP film and the coverage of individual layers during growth can be extracted. It can be seen that layer-by-layer growth persists for the first ∼7 DIP monolayers before roughening sets in.

has been studied in considerable detail. DIP has been shown to exhibit excellent out of plane order [5, 64, 65] and also has been found to have promising charge carrier mobility [49, 66].

Real-time measurements of the x-ray reflectivity for DIP in a wide q-range show the appearance of the first and second order Bragg reflections of DIP (figure 5(b)), evidencing the growth of a DIP structure in which the individual molecules are 'standing upright'. Pronounced side maxima can be seen next to the DIP Bragg reflections (so called Laue fringes), which originate from interference of reflections from the top and bottom surface of the DIP film. The pronounced Laue fringes show that the DIP film surface remains smooth during growth, and consequently growth oscillations are only weakly damped (figure 5(c)). Modelling these growth oscillations again with the kinematic approximation of x-ray scattering and a diffusive growth model (equations (1) and (2)) yields the interface width (roughness) and the individual layer coverages as in the pentacene case. By comparing figures 4(b) and 5(b), it is evident that for DIP the growth oscillations and Laue fringes are less damped and the quantitative analysis in figure 5(d) shows that DIP layer by layer growth persists longer than in pentacene (up to ∼7–8 ML as compared to 4 ML). Also the absolute roughness is significantly lower than that of pentacene. After ∼7 ML roughening sets in for DIP as well, and indeed for thicker films the roughness increases faster than expected for random deposition of molecules. This rapid roughening has been followed to large film thicknesses of 10 000 Å in [5] and has also been found in other organic systems [42].

The reasons for the transition from layer-by-layer growth to roughening are not yet well understood for complex organic molecular materials. Strained growth in the first monolayers and strain relaxation may trigger a change in growth mode, but for organic molecules the molecular tilt angle and the molecular conformation may also change during growth. Differently tilted molecules will have different bulk- and surface energies. Therefore a change in molecular orientation may occur when the balance between bulk- and surface energies changes, such that the bulk contribution surpasses the surface energy contribution at a critical thickness [67].

For DIP, it has been found that the in plane lattice parameter changes during growth of the first three monolayers. Figure 6 shows the evolution of the in plane (11) reflection of DIP, that is the evolution of the lattice parameter parallel to the surface. From figure 6 it can be seen that the in plane lattice parameter of DIP in the first monolayer expands by 2% upon absorption of further layers. The structure actually changes in a collective fashion, that is, the first monolayer

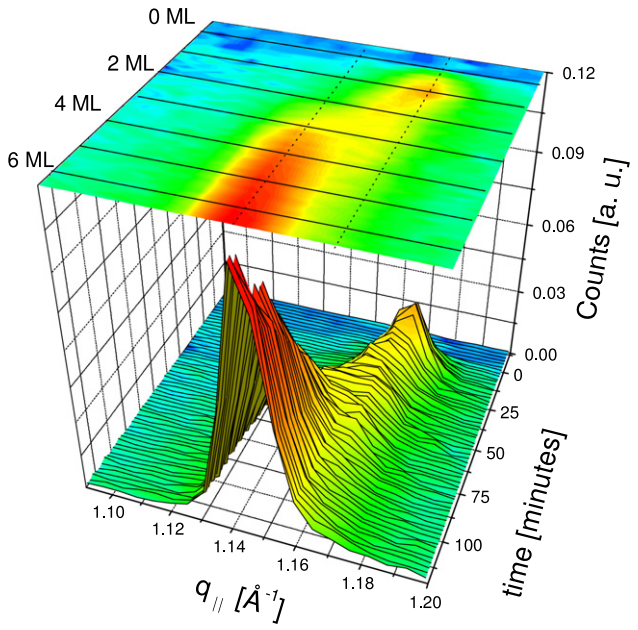

Figure 6. In plane structure: real-time GID scans during growth of DIP on silicon oxide (130 °C). The in plane (11) reflection of the DIP film shifts during growth of the second and third monolayer. After growth of three monolayers the transient structure of the first monolayer has vanished.

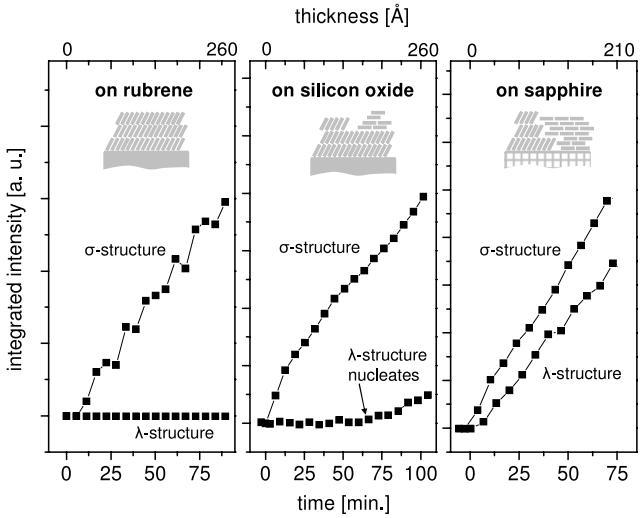

Figure 7. Evolution of the (100) and (11) reflections of DIP as a function of time (film thickness), for growth on rubrene (10 °C), silicon oxide, and stepped sapphire (both at 35 °C). The two reflections are characteristic for two different molecular orientations, that is a lying down (λ) orientation and a standing upright (σ) orientation of the DIP molecules respectively (see the inset). Reprinted figure with permission from [6]. Copyright 2006 by the American Physical Sociey.

exhibits a transient structure. This transient structure would be missed in post-growth measurements. Stopping growth after one monolayer also could not replace real-time measurements, because a single DIP monolayer is not stable and partially dewets on a 10 min timescale. The increase of the lattice constant of the first DIP layers may be explained by strain, but also by a slight change of molecular tilt angle.

Similar to pentacene growth, where a second phase can grow in addition to the thin film phase for certain growth conditions, DIP also exhibits growth of a second structure for low sample temperatures. In addition to the upright standing orientation of the DIP molecules prevalent at 130 °C sample temperature, a second DIP structure starts to grow with molecules lying down at room temperature or lower [6, 68]. This change in molecular orientation does depend on substrate temperature as well as the type of substrate (see figure 7). For growth on silicon oxide at 35 °C, the lying down structure starts to grow after a critical thickness of ∼170 Å, such that the lying down structure grows on top of the standing upright structure of DIP. In contrast, when growing DIP on top of the organic semiconductor rubrene at the same temperature, no lying down structure nucleates. When using A plane sapphire as a substrate, the nucleation of the lying phase occurs without threshold thickness. The substrate dependence of the lying down structure can be rationalized by regarding the substrate interactions with DIP. Rubrene substrates have only weak van der Waals interactions that favour the standing upright structure. In contrast, the stronger effective interaction with sapphire due to the stepped sapphire surface and the slightly higher van der Waals interactions lead to molecules adopting a lying down orientation and therefore the early nucleation of the lying down structure.

3.3. PTCDA/Ag(111)

PTCDA is among the most thoroughly studied organic semiconductors and was considered an OMBD model system [12, 13, 15, 69] (see also x-ray standing wave section including the references therein). One of the characteristic features of PTCDA is that it (almost) always grows in a lying down configuration in contrast to pentacene and DIP, which is probably due to its layered crystal structure and molecular quadrupole moment.

When grown at low substrate temperatures ($T < 50$ °C at a growth rate of 1 Å min^{-1}), PTCDA films exhibit a smooth morphology albeit with poor crystallinity. As is often observed for OMBD, higher substrate temperatures give improved crystallinity, albeit with a rough morphology with separated crystals on a range of substrates such as PTCDA/InAs(001) [70], PTCDA/NaCl(001), KCl(001) and KBr(001) [71], Au(111) [72, 73], and Ag(111) (see [4, 26, 70, 74–78] and references therein). It turned out that PTCDA exhibits very well defined Stranski–Krastanov growth on Ag(111) as established in real-time x-ray experiments.

Figure 8(c) shows x-ray growth oscillations for PTCDA deposition on Ag(111) at different substrate temperatures clearly demonstrating (i) the decay of crystallinity and therefore growth oscillations at low substrate temperatures, and (ii) the damping of oscillations after deposition of two monolayers, indicative of a transition from 2d to 3d growth (Stranski–Krastanov growth with two monolayers wetting). Again fits of the growth oscillations have been performed within the kinematic (single scattering) approximation of x-ray scattering, but in this example kinetic Monte Carlo simulations [79] have been used to model the evolution of the

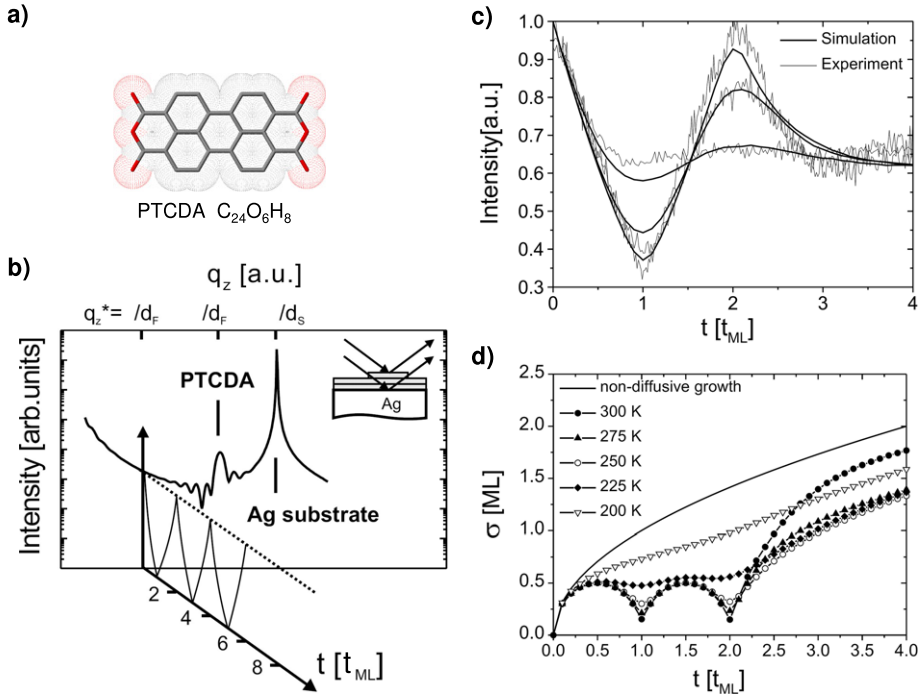

Figure 8. (a) Schematic of the molecule 3,4,9,10-perylenetetracarboxylic dianhydride (PTCDA). (b) Simulation of the specular reflectivity of a PTCDA film on an Ag (111) substrate (from [70]). At the anti-Bragg point of the PTCDA film ($q^*z = \pi/d_F$), the scattering of subsequent layers interferes destructively, so that during film growth the reflected intensity at the anti-Bragg point oscillates as a function of the deposition time. (c) Comparison between experimental anti-Bragg oscillations (substrate temperatures 233, 303, and 358 K) and Monte Carlo simulations (simulations at 200, 225, 250 K). (d) Interface roughness as obtained from Monte Carlo simulations at different temperatures. Clearly a transition from 2d to 3d growth is visible after two monolayers at high temperatures, which for low temperatures (200 K) occurs as early as after half a monolayer deposition. Reprinted figures with permission from [70].

layer coverages $\theta_n(t)$. While temperatures for the calculations systematically lie below the real substrate temperature, indicating that the energy barriers in the calculations are slightly too low, the x-ray growth oscillations are fitted well. This allows a calculation of the film roughness σ from the simulated $\theta_n(t)$ as shown in figure 8(d). At high substrate temperatures the first two layers grow in a well defined layer-by-layer fashion with a pronounced transition to island growth after two monolayers. The layer-by-layer growth of the first layers is strongly temperature dependent and breaks down for lower substrate temperatures.

4. A closer look at the first monolayer

It has been demonstrated that the first monolayer forms a crucial template for the growth of further molecular layers [13, 15]. Therefore, the strength of the adsorbate–substrate interaction, the orientation of the molecules, their bonding distances, d_0, to the topmost substrate layer (see figure 1) determine to some extent the properties of a multilayer thin film. Particularly, the alignment of energy levels at the organic interface and the resulting efficiency of charge injection from metal contacts is affected by the monolayer structure and the related effects such as molecular distortions and distortion induced molecular dipoles. Further details on the electronic properties of organic adsorbates can be found in the review by Koch in this issue.

The (average) bonding distance d_0 of the monolayer is the central quantity in this context and already emerged in the real-time experiments discussed above where it was determined from x-ray scans on the specular path [4]. More precise and chemically resolved structural information, however, can be obtained from x-ray standing wave (XSW) experiments [80–82]. Following the early experiments on simple adsorption systems, the XSW technique has recently been used to study larger, conjugated organic molecules adsorbed on metal surfaces [8, 9, 83–87].

As a basically interferometric approach, the XSW technique works as follows (see figure 9): An x-ray standing wave field with the periodicity of the substrate lattice d_{hkl} is generated by Bragg reflection from a single crystal that also serves as substrate for the organic film. By scanning the photon energy E of the incident wave through the Bragg condition the phase of the interference field changes by π and, as a consequence, the nodal planes of the standing wave field shift by half a lattice constant. Since the absorption of x-rays depends on the position of the atoms within this wave field, photoelectrons (or, for heavier elements, also x-ray fluorescence) can be used as element specific signals, which reveal the position of the adsorbate atoms. The measured photoelectron yield $Y_p(E)$ exhibits a characteristic shape that can be related to the bonding distance d_0 of a given chemical element. Due to the high spatial resolution of typically $\leqslant$0.05 Å XSW measurements probe the molecular geometry with high precision.

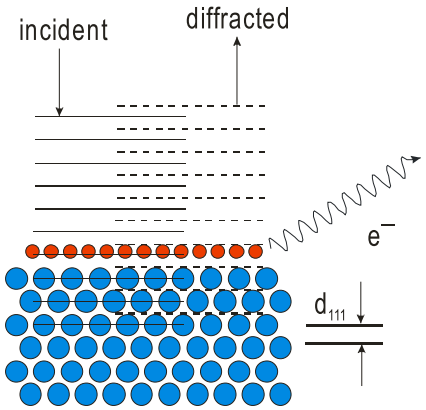

Figure 9. XSW principle. The standing wave field is produced by Bragg reflection of monochromatic x-rays from a single crystal substrate. The variation of the photoelectron yield when scanning the photon energy through the Bragg condition depends on the adsorbate position d_0. Note, that XSW measurements with XPS detection determine the initial state geometry of the molecules, since any possible nuclear relaxation after ionization is slower than the photoemission process (for details see [88]).

Below we shall discuss a number of experimental results that demonstrate adsorption distances d_0 deduced from XSW measurements provide significant insight into the complex substrate–adsorbate interaction.

4.1. PTCDA/Ag(111), Cu(111), and Au(111)

PTCDA has become the best studied system in this field, see e.g. [4, 26, 74, 89, 90]. There are precise data on three different substrates, i.e. Ag(111), Cu(111), and Au(111) as shown in figure 10 and table 1. A strong interaction with the substrates ('chemisorption') is found for Ag(111) and Cu(111) with a bonding distance of 2.86±0.01 Å [8, 84] and 2.61±0.02 Å [8], respectively. Yet, a much weaker interaction is found for PTCDA on Au(111) with 3.27 ± 0.02 Å [91]. The close correlation of these findings with the electronic properties of PTCDA on the different substrates is discussed in [10].

The XSW results of PTCDA/Ag(111) obtained in the monolayer regime agree with surface diffraction data obtained from multilayer films of PTCDA [4]. This indicates that the growth of further layers does not influence the first layer and the XSW measurements of d_0 discussed here are indeed relevant beyond the monolayer coverage. Moreover, a substrate dependent distortion of the C=O bonds is found: for PTCDA on Ag(111) the carboxylic oxygen atoms are located below the molecular plane ($d_0 = 2.68$ Å), but for PTCDA on Cu(111) these atoms are *above* the plane ($d_0 = 2.73$ Å), see figure 2. Theoretical efforts based mainly on density functional theory are being made to explain these findings, but are still hampered by the necessarily tedious computations.

Table 1. Bonding distances d_0 on Cu(111) and Ag(111) measured with the XSW technique. The values correspond to the (average) carbon distance relative to the Bragg planes of the substrate.

	Cu(111)	Ag(111)	Au(111)
PTCDA	2.66 ± 0.02 Å	2.86 ± 0.01 Å	3.27 ± 0.02 Å
NTCDA		2.997 ± 0.016 Å	
F_{16}CuPc	2.61 ± 0.05 Å	3.25 ± 0.05 Å	
SnPc (prepared by desorption)		3.17 ± 0.03 Å	
SnPc (prepared at 300 °C)		3.61 ± 0.16 Å	

4.2. NTCDA/Ag(111)

Recent XSW experiments [83, 86] demonstrate that the adsorption geometry of NTCDA on Ag(111) is similar to the one found for the larger PTCDA molecule. A slightly weaker substrate–adsorbate interaction results in a carbon distance of $d_0 = 2.997 \pm 0.016$ Å to the Ag(111) lattice. Therefore, the adsorption of NTCDA might be regarded as relatively strong (chemisorption). A non-planar adsorption geometry is also reported for NTCDA [86]. In essence, the distortion of the C=O bonds in NTCDA is similar to the case of PTCDA on Ag(111) in which the carboxylic oxygen atoms are located below the molecular plane. Since no XSW data for Cu(111) or Au(111) are presently available, a substrate dependent distortion of NTCDA—as found for PTCDA—has not yet been established.

4.3. F_{16}CuPc/Ag (111) and Cu(111)

The XSW results obtained on F_{16}CuPc show that perfluorinated copper–phthalocyanine molecules adsorb in a lying down, but significantly distorted configuration on Cu(111) and Ag(111) surfaces [9]. While on copper (silver) the central carbon rings reside 2.61 ± 0.05 Å (3.25 ± 0.05 Å) above the substrate, the outer fluorine atoms are located 0.27 Å (0.20 Å) further away from the surface. These results on F_{16}CuPc are in remarkable contrast to those on PTCDA on Cu(111) and Ag(111)

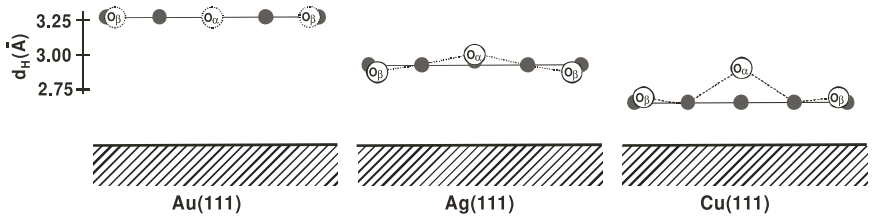

Figure 10. Different bonding distances and adsorption geometries of PTCDA on Au(111), Ag(111) and Cu(111) as measured by XSW [8, 84, 91]. On copper both oxygen species—distinguishable due to a chemical shift in the photoemission spectra—are located above the carbon plane. On silver, however, the carboxylic oxygen atoms are bent towards the surface. The position of the oxygen atoms on gold was not measured with XSW. From [10] with permission.

mentioned above. First, a much larger difference between the adsorption distances d_0 on copper and silver is found. Second, the type of molecular distortion, i.e. an upward bending of the C–F bonds in F_{16}CuPc, is the same on copper and silver despite the obviously weaker interaction of F_{16}CuPc with the Ag(111) surface. As for PTCDA a thorough explanation for the non-planar adsorption structure of the molecules is still missing. Yet, in [9] it is suggested that the results can be discussed in terms of the outer carbon atoms in F_{16}CuPc undergoing a partial re-hybridization ($sp^2 \rightarrow sp^3$) with a concomitant change of the bonding angles.

4.4. SnPc/Ag(111)

The adsorption geometry and orientation of the non-planar phthalocyanine molecule SnPc has been measured by XSW [85, 87]. Depending on the preparation conditions SnPc monolayers exhibit different superstructures and molecular conformations on the Ag(111) surface. For deposition at 300 °C substrate temperature the carbon atoms are bent away from the surface [87], whereas for a monolayer of SnPc prepared via desorption of a multilayer film the carbon atoms are bent towards the surface [85]. This finding is reflected by the different (averaged) carbon distances found for these conformations of SnPc on Ag(111), i.e., 3.61 ± 0.16 Å [87] versus 3.17 ± 0.03 Å [85].

To conclude, a rich phenomenology of different adsorption behaviours has been found by XSW measurements for examples described above. The strength of the substrate–adsorbate interaction—even for lying down molecules—varies considerably as is demonstrated by the different bonding distances d_0 (table 1). Adsorption induced distortion of the molecules seems to be the rule rather than the exception. Therefore, further studies are required to fully understand the bonding of these systems.

5. Conclusions

Organic molecular beam deposition is a complex topic where growth experiments as well as growth theory are needed for an understanding of the many facets governing the structure formation of organics. We have not attempted to provide a complete overview of the field or a comprehensive account of the literature, for which we refer the reader to earlier reviews [12, 13, 15], but rather we have provided an update on specific issues. In this review we have focused on two aspects we believe are crucial, namely *real-time* effects including structure and strain as a function of time (that is film thickness) and secondly high precision investigations of the first monolayer (mostly using XSW). Of course many more issues arise in the growth of organic molecules with their orientational, conformational and vibrational degrees of freedom, and this is still an open field of research.

Acknowledgments

We wish to thank the many students, collaborators, and colleagues who contributed in various ways to the work reviewed here. We wish to acknowledge discussions with J Engstrom and A Amassian, valuable comments on the manuscript by E Oberla, and financial support from the Deutsche Forschungsgemeinschaft (Focus Programme 'Organic Field-Effect Transistors', Germany) and the EPSRC (UK).

References

[1] Koch N 2008 *J. Phys.: Condens. Matter* **20** 184008
[2] Mannsfeld S C B and Fritz T 2006 Advanced modelling of epitaxial ordering of organic layers on crystalline surfaces *Mod. Phys. Lett.* B **20** 585–605
[3] Käfer D, Ruppel L, Witte G and Wöll C 2005 Role of molecular conformations in rubrene thin film growth *Phys. Rev. Lett.* **95** 166602
[4] Krause B, Dürr A C, Schreiber F, Dosch H and Seeck O H 2003 Thermal stability and partial dewetting of crystalline organic thin films: 3,4,9,10-perylenetetracarboxylic dianhydride on Ag(111) *J. Chem. Phys.* **119** 3429–35
[5] Dürr A C, Schreiber F, Ritley K A, Kruppa V, Krug J, Dosch H and Struth B 2003 Rapid roughening in thin film growth of an organic semiconductor (diindenoperylene) *Phys. Rev. Lett.* **90** 016104
[6] Kowarik S, Gerlach A, Sellner S, Schreiber F, Cavalcanti L and Konovalov O 2006 Real-time observation of structural and orientational transitions during growth of organic thin films *Phys. Rev. Lett.* **96** 125504
[7] Wang L, Qi D C, Liu L, Chen S, Gao X Y and Wee A T S 2007 Molecular orientation and ordering during initial growth of copper phthalocyanine on Si(111) *J. Phys. Chem.* C **111** 3454–8
[8] Gerlach A, Sellner S, Schreiber F, Koch N and Zegenhagen J 2007 Substrate dependent bonding distances of PTCDA—a comparative x-ray standing wave study on Cu(111) and Ag(111) *Phys. Rev.* B **75** 045401
[9] Gerlach A, Schreiber F, Sellner S, Dosch H, Vartanyants I A, Cowie B C C, Lee T-L and Zegenhagen J 2005 Adsorption-induced distortion of F_{16}CuPc on Cu(111) and Ag(111): an x-ray standing wave study *Phys. Rev.* B **71** 205425
[10] Duhm S, Gerlach A, Salzmann I, Bröcker B, Johnson R L, Schreiber F and Koch N 2007 PTCDA on Au(111), Ag(111) and Cu(111): correlating bonding distance and interfacial charge transfer *Org. Electron.* at press
[11] Koma A 1995 Molecular-beam epitaxial-growth of organic thin-films *Prog. Cryst. Growth Charact. Mater.* **30** 129–52
[12] Forrest S R 1997 Ultrathin organic films grown by organic molecular beam deposition and related techniques *Chem. Rev.* **97** 1793–896
[13] Schreiber F 2004 Organic molecular beam deposition: growth studies beyond the first monolayer *Phys. Status Solidi* a **201** 1037–54
[14] Fraxedas J 2002 Perspectives on thin molecular organic films *Adv. Mater.* **14** 1603–14
[15] Witte G and Wöll C 2004 Growth of aromatic molecules on solid substrates for applications in organic electronics *J. Mater. Res.* **19** 1889–916
[16] Dimitrakopoulos C D and Malenfant P R L 2002 Organic thin film transistors for large area electronics *Adv. Mater.* 99–117
[17] Brütting W E 2005 *Physics of Organic Semiconductors* (New York: Wiley–VCH)
[18] Markov I V 2004 *Crystal Growth for Beginners* 2nd edn (Singapore: World Scientific)
[19] Krug J and Michely T 2004 *Islands, Mounds and Atoms: Patterns and Processes in Crystal Growth Far From Equilibrium* (Berlin: Springer)

[20] Pimpinelli A and Villain J 1998 *Physics of Crystal Growth* (Cambridge: Cambridge University Press)

[21] Barabási A-L and Stanley H E 1995 *Fractal Concepts in Surface Growth* (Cambridge: Cambridge University Press)

[22] Jackson K A 2004 *Kinetic Processes: Crystal Growth, Diffusion, and Phase Transformations in Materials* (New York: Wiley)

[23] Jackson K A 2002 The interface kinetics of crystal growth processes *Interface Sci.* **10** 159–69

[24] Tromp R M and Hannon J B 2002 Thermodynamics of nucleation and growth *Surf. Rev. Lett.* **9** 1565–93

[25] Venables J A, Spiller G D T and Hanbücken M 1984 Nucleation and growth of thin films *Rep. Prog. Phys.* **47** 399–459

[26] Krause B, Durr A C, Schreiber F, Dosch H and Seeck O H 2004 Late growth stages and post-growth diffusion in organic epitaxy: PTCDA on Ag(1 1 1) *Surf. Sci.* **572** 385–95

[27] Beernink G, Strunskus T, Witte G and Wöll C 2004 Importance of dewetting in organic molecular-beam deposition: pentacene on gold *Appl. Phys. Lett.* **85** 398–400

[28] Yoshikawa G, Sadowski J T, Al-Mahboob A, Fujikawa Y, Sakurai T, Tsuruma Y, Ikeda S and Saiki K 2007 Spontaneous aggregation of pentacene molecules and its influence on field effect mobility *Appl. Phys. Lett.* **90** 251906

[29] Hoshino A, Isoda S and Kobayashi T 1991 Epitaxial growth of organic crystals on organic substrates–polynuclear aromatic hydrocarbons *J. Cryst. Growth* **115** 826–30

[30] Hooks D E, Fritz T and Ward M D 2001 Epitaxy and molecular organization on solid substrates *Adv. Mater.* **13** 227–41

[31] Gerstenberg M C, Schreiber F, Leung T Y B, Bracco G, Forrest S R and Scoles G 2000 Organic semiconducting thin film growth on an organic substrate: 3,4,9,10-perylenetetracarboxylic dianhydride on a monolayer of decanethiol self-assembled on Au(111) *Phys. Rev.* B **61** 7678–85

[32] Schreiber F, Gerstenberg M C, Dosch H and Scoles G 2003 Melting point enhancement of a self-assembled monolayer induced by a van der Waals bound capping layer *Langmuir* **19** 10004–6

[33] Schreiber F, Gerstenberg M C, Edinger B, Toperverg B, Forrest S R, Scoles G and Dosch H 2000 Phase-sensitive surface x-ray scattering study of a crystalline organic–organic heterostructure *Physica* B **283** 75–8

[34] Killampalli A S and Engstrom J R 2006 Nucleation of pentacene thin films on silicon dioxide modified with hexamethyldisilazane *Appl. Phys. Lett.* **88** 143125

[35] Käfer D, Ruppel L and Witte G 2007 Growth of pentacene on clean and modified gold surfaces *Phys. Rev.* B **75** 085309

[36] Ruiz R, Nickel B, Koch N, Feldman L C, Haglund R F, Kahn A and Scoles G 2003 Pentacene ultrathin film formation on reduced and oxidized Si surfaces *Phys. Rev.* B **67** 125406

[37] Klauk H, Zschieschang U, Pflaum J and Halik M 2007 Ultralow-power organic complementary circuits *Nature* **445** 745–8

[38] Aumann C E, Kariotis R and Lagally M G 1989 Rate equation modeling of interface width *J. Vac. Sci. Technol.* A **7** 2180–5

[39] Krug J 1997 Origins of scale invariance in growth processes *Adv. Phys.* **46** 139–282

[40] Krug J 2004 Power laws in surface physics: the deep, the shallow and the useful *Preprint* cond-mat/0403267 v1

[41] Ruiz R, Nickel B, Koch N, Feldman L C, Haglund R F Jr, Kahn A, Family F and Scoles G 2003 Dynamic scaling, island size distribution, and morphology in the aggregation regime of submonolayer pentacene films *Phys. Rev. Lett.* **91** 136102

[42] Yim S and Jones T S 2006 Anomalous scaling behavior and surface roughening in molecular thin-film deposition *Phys. Rev.* B **73** 161305(R)

[43] Lafouresse M C, Heard P J and Schwarzacher W 2007 Anomalous scaling for thick electrodeposited films *Phys. Rev. Lett.* **98** 236101

[44] Kowarik S, Gerlach A, Sellner S, Schreiber F, Pflaum J, Cavalcanti L and Konovalov O 2006 Anomalous roughness evolution of rubrene thin films observed in real time during growth *Phys. Chem. Chem. Phys.* **8** 1834–6

[45] Meyer zu Heringdorf F J, Reuter M C and Tromp R M 2001 Growth dynamics of pentacene thin films *Nature* **412** 517–20

[46] Braun W, Däweritz L and Ploog K H 1998 Origin of electron diffraction oscillations during crystal growth *Phys. Rev. Lett.* **80** 4935–8

[47] Casalis L, Danisman M F, Nickel B, Bracco G, Toccoli T, Iannotta S and Scoles G 2003 Hyperthermal molecular beam deposition of highly ordered organic thin films *Phys. Rev. Lett.* **90** 206101

[48] Söhnchen S, Lukas S and Witte G 2004 Epitaxial growth of pentacene films on Cu(110) *J. Chem. Phys.* **121** 525–34

[49] Karl N 2001 Organic electronic materials *Organic Electronic Materials* ed R Farchioni and G Grosso (Berlin: Springer)

[50] Ruiz R, Mayer A C, Malliaras G G, Nickel B, Scoles G, Kazimirov A, Kim H, Headrick R L and Islam Z 2004 Structure of pentacene thin films *Appl. Phys. Lett.* **85** 4926–8

[51] Ruiz R, Choudhary D, Nickel B, Toccoli T, Chang K-C, Mayer A C, Clancy P, Blakely J M, Headrick R L, Iannotta S and Malliaras G G 2004 Pentacene thin film growth *Chem. Mater.* **16** 4497–508

[52] Yoshida H, Inaba K and Sato N 2007 X-ray diffraction reciprocal space mapping study of the thin film phase of pentacene *Appl. Phys. Lett.* **90** 181930

[53] Schiefer S, Huth M, Dobrinevski A and Nickel B 2007 Determination of the crystal structure of substrate-induced pentacene polymorphs in fiber structured thin films *J. Am. Chem. Soc.* **129** 10316–7

[54] Pratontep S, Brinkmann M, Nuesch F and Zuppiroli L 2004 Correlated growth in ultrathin pentacene films on silicon oxide: effect of deposition rate *Phys. Rev.* B **69** 165201

[55] Killampalli A S, Schroeder T W and Engstrom J R 2005 Nucleation of pentacene on silicon dioxide at hyperthermal energies *Appl. Phys. Lett.* **87** 033110

[56] Mayer A C, Kazimirov A and Malliaras G G 2006 Dynamics of bimodal growth in pentacene thin films *Phys. Rev. Lett.* **97** 105503

[57] Mayer A C, Ruiz R, Headrick R L, Kazimirov A and Malliaras G G 2004 Early stages of pentacene film growth on silicon oxide *Org. Electron.* **5** 257–63

[58] Mayer A C, Ruiz R, Zhou H, Headrick R L, Kazimirov A and Malliaras G G 2006 Growth dynamics of pentacene thin films: real-time synchrotron x-ray scattering study *Phys. Rev.* B **73** 205307

[59] Kowarik S, Gerlach A, Leitenberger W, Hu J, Witte G, Wöll C, Pietsch U and Schreiber F 2007 Energy-dispersive x-ray reflectivity and GID for real-time growth studies of pentacene thin films *Thin Solid Films* **515** 5606–10

[60] Bouchoms I P M, Schoonveld W A, Vrijmoeth J and Klapwijk T M 1999 Morphology identification of the thin film phases of vacuum evaporated pentacene on SiO_2 substrates *Synth. Met.* **104** 175–8

[61] Kowarik S, Gerlach A, Skoda M, Sellner S and Schreiber F 2008 Real-time studies of thin film growth: measurement and analysis of x-ray growth oscillations beyond the anti-Bragg point, submitted

[62] Cohen P I, Petrich G S, Pukite P R, Whaley G J and Arrott A S 1989 Birth–death models of epitaxy: I. Diffraction oscillations from low index surfaces *Surf. Sci.* **216** 222–48

[63] Markov I V 1994 *Crystal Growth for Beginners: Fundamentals of Nucleation, Crystal Growth and Epitaxy* (Singapore: World Scientific)

[64] Dürr A C, Schreiber F, Kelsch M and Dosch H 2003 Optimized preparation of cross-sectional TEM specimens of organic thin films *Ultramicroscopy* **98** 51–5
[65] Dürr A C, Schreiber F, Munch M, Karl N, Krause B, Kruppa V and Dosch H 2002 High structural order in thin films of the organic semiconductor diindenoperylene *Appl. Phys. Lett.* **81** 2276–8
[66] Münch M 2001 Strukturelle Beeinflussung der elektrischen Transporteigenschaften dünner organischer Schichten *PhD Thesis* Universität Stuttgart
[67] Drummy L F and Martin D C 2005 Thickness-driven orthorhombic to triclinic phase transformation in pentacene thin films *Adv. Mater.* **17** 903–7
[68] Dürr A C, Nickel B, Sharma V, Taffner U and Dosch H 2006 Observation of competing modes in the growth of diindenoperylene on SiO_2 *Thin Solid Films* **503** 127–32
[69] Umbach E 1991 Characterization of organic overlayers on well defined substrates *Prog. Surf. Sci.* **35** 113–27
[70] Krause B, Schreiber F, Dosch H, Pimpinelli A and Seeck O H 2004 Temperature dependence of the 2D–3D transition in the growth of PTCDA on Ag(111): a real-time x-ray and kinetic Monte Carlo study *Europhys. Lett.* **65** 372–8
[71] Schlettwein D, Back A, Schilling B, Friz T and Armstrong N R 1998 Ultrathin films of perylenedianhydride and perylenebis(dicarboximide) dyes on (001) alkali halide surfaces *Chem. Mater.* **10** 601–12
[72] Kilian L, Umbach E and Sokolowski M 2006 A refined structural analysis of the PTCDA monolayer on the reconstructed Au(111) surface—'Rigid or distorted carpet?' *Surf. Sci.* **600** 2633–43
[73] Fenter P, Schreiber F, Zhou L, Eisenberger P and Forrest S R 1997 *In situ* studies of morphology, strain, and growth modes of a molecular organic thin film *Phys. Rev.* B **56** 3046–53
[74] Krause B, Dürr A C, Ritley K, Schreiber F, Dosch H and Smilgies D 2002 Structure and growth morphology of an archetypal system for organic epitaxy: PTCDA on Ag(111) *Phys. Rev.* B **66** 235404
[75] Krause B, Dürr A C, Ritley K A, Schreiber F, Dosch H and Smilgies D 2001 On the coexistence of different polymorphs in organic epitaxy: alpha and beta phase of PTCDA on Ag(111) *Appl. Surf. Sci.* **175** 332–6
[76] Krause B 2002 Growth and structure of the organic molecule PTCDA on Ag(111) *PhD Thesis* Universität Stuttgart
[77] Kilian L, Umbach E and Sokolowski M 2004 Molecular beam epitaxy of organic films investigated by high resolution low energy electron diffraction (SPA-LEED): 3,4,9,10-perylenetetracarboxylicacid-dianhydride (PTCDA) on Ag(111) *Surf. Sci.* **573** 359–78
[78] Eremtchenko M, Schaefer J A and Tautz F S 2003 Understanding and tuning the epitaxy of large aromatic adsorbates by molecular design *Nature* **425** 602–5
[79] Tan S and Lam P M 1999 Monte Carlo simulation of three-dimensional islands *Phys. Rev.* B **60** 8314–20
[80] Zegenhagen J 1993 Surface structure determination with x-ray standing waves *Surf. Sci. Rep.* **18** 199
[81] Bedzyk M J and Cheng L 2002 X-ray standing wave studies of minerals and mineral surfaces; principles and applications *Rev. Mineral. Geochem.* **49** 221
[82] Woodruff D P 2005 Surface structure determination using x-ray standing waves *Rep. Prog. Phys.* **68** 743
[83] Stanzel J, Weigand W, Kilian L, Meyerheim H L, Kumpf C and Umbach E 2004 Chemisorption of NTCDA on Ag(111): a NIXSW study including non-dipolar and electron-stimulated effects *Surf. Sci. Lett.* **571** 311
[84] Hauschild A, Karki K, Cowie B C C, Rohlfing M, Tautz F S and Sokolowski M 2005 Molecular distortions and chemical bonding of a large Pi-conjugated molecule on a metal surface *Phys. Rev. Lett.* **94** 36106
[85] Stadler C, Hansen S, Pollinger F, Kumpf C, Umbach E, Lee T-L and Zegenhagen J 2006 Structural investigation of the adsorption of SnPc on Ag(111) using normal-incidence x-ray standing waves *Phys. Rev.* B **74** 035404
[86] Stadler C, Hansen S, Schöll A, Lee T-L, Zegenhagen J, Kumpf C and Umbach E 2007 Molecular distortion of NTCDA upon adsorption on Ag(111): a normal incidence x-ray standing wave study *New J. Phys.* **9** 50
[87] Woolley R A J, Martin C P, Miller G, Dhanak V R and Moriarty P J 2007 Adsorbed molecular shuttlecocks: an NIXSW study of Sn phthalocyanine on Ag(111) using Auger electron detection *Surf. Sci.* **601** 1231
[88] Schreiber F, Gerlach A, Koch N, Zojer E, Sokolowski M, Tautz F S, Rohlfing M and Umbach E 2007 Comment on 'electron core–hole interaction and its induced ionic structural relaxation in molecular systems under x-ray irradiation' *Phys. Rev. Lett.* **99** 059601
[89] Kilian L, Umbach E and Sokolowski M 2004 Molecular beam epitaxy of organic films investigated by high resolution low energy electron diffraction (SPA-LEED): 3,4,9,10-perylenetetracarboxylicacid-dianhydride (PTCDA) on Ag(111) *Surf. Sci.* **573** 359–78
[90] Zou Y, Kilian L, Schöll A, Schmidt T, Fink R and Umbach E 2006 Chemical bonding of PTCDA on Ag surfaces and the formation of interface states *Surf. Sci.* **600** 1240
[91] Henze S K M, Bauer O, Lee T-L, Sokolowski M and Tautz F S 2007 Vertical bonding distances of PTCDA on Au(111) and Ag(111): Relation to the bonding type *Surf. Sci.* **601** 1566–73